

EXTRACTION OF THE DEFECT DENSITY OF STATES OF A-SI:H USING Q-DLTS

B.E. Pieters, M. Zeman, W.J. Metselaar.

Delft University of Technology, Laboratory of Electronic Components, Technology and Materials - DIMES

P.O. Box 5053, NL-2600 GB Delft, the Netherlands

Phone: +31 (0)15 278 1651 Fax: +31 (0)15 262 2163

E-mail: B.E.Pieters@its.tudelft.nl

Abstract—Q-DLTS is a powerful tool for the investigation of the defect-state distribution in hydrogenated amorphous silicon (*a*-Si:H). In this work we have adapted our device simulator ASA to be able to simulate metal/insulator/semiconductor (MIS) structures. With this new version of ASA we can directly simulate Q-DLTS signals. A good correspondence between simulated and experimental Q-DLTS results was obtained. Using these simulations we have extracted the defect-state density for the measured *a*-Si:H sample. The spatial sensitivity of the Q-DLTS signal as a function of temperature was studied. It was shown that more than 90% of the signal comes from a region of less than 100nm wide adjacent to the oxide/semiconductor interface of the sample. The Q-DLTS signal at temperatures below 250°K and at temperatures above 350°K is dominated by a relatively thin region (more than 60% of the signal comes from the first 10 nm). The influence of a defective *a*-Si:H layer at the SiO_x/*a*-Si:H interface on the spatial sensitivity of Q-DLTS was studied.

Keywords—charge deep level transient spectroscopy, amorphous silicon, simulation, modelling, density of states

I. INTRODUCTION

The distribution of defect states in the energy gap of *a*-Si:H is an important parameter for the modelling of *a*-Si:H solar cells. For the characterisation of the distribution of defects states in the bandgap, deep-level transient spectroscopy (DLTS) [1], can be used.

DLTS is a widely accepted technique for detecting electrically active traps. In this technique the change in capacitance of a Schottky barrier upon a bias pulse is measured. By taking the energy and temperature dependence of the emission rates of traps in the semiconductor, the density of defect states within the gap can be reconstructed from the transient of the capacitance. Generally the capacitance transient is measured with a fast capacitance meter. However, it is possible to use the current or charge transients instead. The charge and current DLTS techniques have the advantage over capacitance DLTS that they can be used for the characterisation of undoped *a*-Si:H samples. Compared to capacitance DLTS, charge and current DLTS are much more sensitive to the interface density of states. Charge and current DLTS suffer from their sensitivity to leakage currents and are therefore measured on MIS structures. The current DLTS method suffers from amplitude loss when slow charge release from deep traps is measured. For this reason we applied

the charge DLTS (Q-DLTS) method.

A procedure for extracting the density of states distribution in energy and space from the Q-DLTS response was developed by Nádaždy and Thurzo [2]. However, this model is less suitable for undoped materials as it requires an accurate estimation of the width and amount of band-bending in the sample.

For an exact evaluation of the Q-DLTS signal the Poisson equation needs to be solved for a MIS structure, and a double integral over both spatial and energy coordinates needs to be evaluated. To do this we adapted our device simulator ASA to be able to simulate MIS structures. Using this new version of ASA we can simulate Q-DLTS signals taking into account the spatial distribution of defects, band tail states and amphoteric defect states [3]. Furthermore, the model can be combined with several defect pool models [4–6] or with a Gaussian distribution of defect states.

In this work we compared experimental Q-DLTS results with the model. By calibrating the model to the experimental results the defect distribution in energy and space was extracted. As Q-DLTS is more sensitive to defects at the insulator/semiconductor interface, the spatial sensitivity was studied. The influence of a defective Si layer at the SiO_x/*a*-Si:H interface on the spatial sensitivity was studied.

II. CHARGE DEEP-LEVEL TRANSIENT SPECTROSCOPY

A. Theoretical Background

In DLTS measurements the transient response of the capacitance of a Schottky barrier or a MIS structure to a bias pulse is measured. The bias pulse is used to fill the traps within the bandgap with electrons. The probability that a trapped electron escapes to the conduction band strongly depends on the energy level at which it is trapped. For this reason the emission rate of trapped electrons, is much higher for electrons trapped at shallow defects than for electrons trapped at deep defects. Therefore the capacitance shows a transient. The emission rate of an electron, trapped at a defect at energy E below the conduction band edge E_c , is given by:

$$e_n(E, T) = e_0(E, T) \exp\left(-\frac{E}{kT}\right) \quad (1)$$

In *a*-Si:H the prefactor e_0 follows the Myer-Neldel relation (MNR) [7].

$$e_0(E, T) = e_{00}(T) \exp\left(\frac{E}{E_0}\right) \quad (2)$$

The temperature dependence of e_{00} is assumed to be small compared to the exponential term in Eq. 1. From Eq. 1 it follows that the emission rate of electrons to the conduction band increases with temperature.

In a Q-DLTS measurement the charge release of a MIS structure after a filling pulse is measured as a function of temperature. By applying a time constant filter (TCF), only charge release at a certain emission rates is measured. We will refer to this rate as *filter rate*. This way the measured charge release at low temperatures corresponds with charge released from shallow defects and the charge measured at high temperatures corresponds with charge released from deep levels.

After the end of the filling pulse the charge that is released from the sample over a time interval, $[t_1, t_2]$, can be computed with:

$$\Delta Q(T) = qA \int_0^d \int_{E_v}^{E_c} N(E, x) \Delta f(E, x) K(E, T) dE dx, \quad (3)$$

where $K(E, T)$ is the first order TCF function:

$$K(E, T) = e^{-t_1 e_n(E, T)} - e^{-t_2 e_n(E, T)}, \quad (4)$$

Δf is the change in occupation probability N is the density states, A is the area of the contact, and q is the elementary charge.

B. Experimental Setup

Fig. 1 shows the experimental setup. The Q-DLTS setup consists of a vacuum chamber to avoid noise in the measurement and the formation of water and ice that might short circuit the sample. The sample holder can be cooled with liquid nitrogen and heated with a heating resistor. A bias voltage can be applied to the top contact of the sample and the chamber and sample holder are grounded.

A schematic drawing of a Q-DLTS sample is shown in Fig. 2. It consists of a Cr/Au back contact, n^+ -type crystalline silicon, $1\mu\text{m}$ $a\text{-Si:H}$, a thin layer of SiO_x (approx. 5 – 8nm) and an aluminium top contact.

The basic circuit of the charge sensitive amplifier used in the Q-DLTS setup, is shown in Fig. 3. During the measurement a bias pulse is applied to fill the defects in the $a\text{-Si:H}$ with electrons. After the pulse a reverse bias is applied to let the electrons be released. The released charge is integrated by the integrating amplifier formed by C_f and the opamp. During the filling pulse the switch S is closed to reset the integrating amplifier. The output signal is sampled at t_1 and $t_2 = 2t_1$. The Q-DLTS signal is the integrated charge release over this interval.

The schematic band diagrams of a Q-DLTS sample with the filling pulse and the negative bias voltage applied are shown in Fig. 4. The purple area in the right picture indicates the traps for which the measurement is most sensitive.

C. Simulation of Q-DLTS signals with ASA

We adapted our device simulator Advanced Semiconductor Analysis (ASA) [8] to directly simulate the Q-DLTS signal of a MIS structure. In order to simulate the Q-DLTS signal the Poisson equation is solved and the double integral from Eq. 3 is

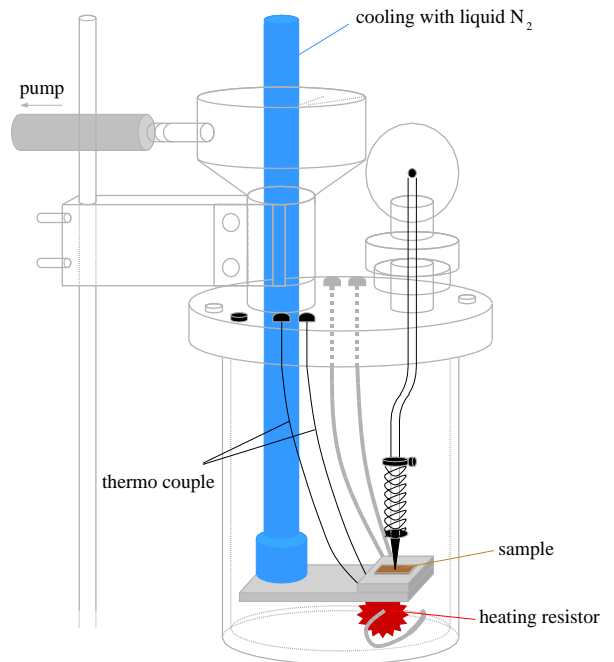


Fig. 1. Schematic drawing of the Q-DLTS setup.

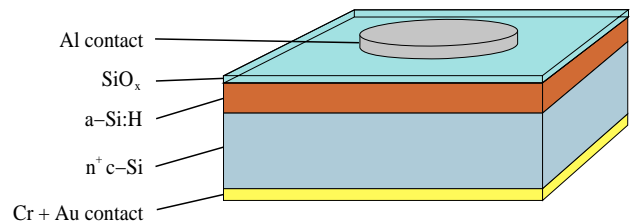


Fig. 2. Schematic picture of a Q-DLTS sample

evaluated. The Q-DLTS signal is computed taking into account tail states and amphoteric defect states in the $a\text{-Si:H}$ layer.

The main features of the ASA program include: (i) calculation of the light generation profile, taking into account both diffuse and coherent light propagation; (ii) models describing a complete density of states distribution as function of energy, which include both the extended and localised (tail and defect) states with corresponding recombination-generation statistics; (iii) calculation of the defect-state distribution in a layer according to the defect-pool models; (iv) a model for the tunnel-recombination junction that allows to simulate a multi-junction $a\text{-Si:H}$ solar cell as one structure; (v) the continuous change (grading) of all input parameters as a function of position in the device can be defined.

III. RESULTS

A. Extraction of the Defect Density of States of $a\text{-Si:H}$

In order to extract the density of states distribution in $a\text{-Si:H}$ the Q-DLTS signal of an $a\text{-Si:H}$ MOS structure was measured and compared to simulations. In the simulations we assumed the defect-pool-model from 1996 [5]. The measurements were

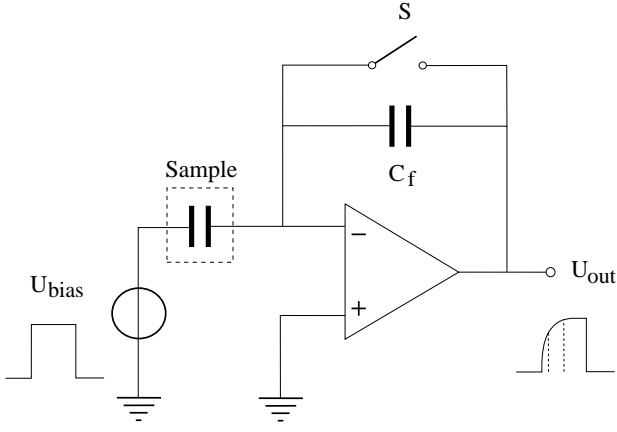


Fig. 3. Schematic circuit of Q-DLTS setup

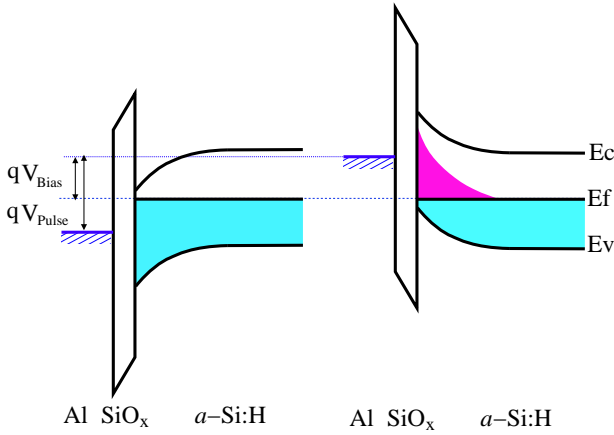


Fig. 4. Schematic band diagrams of an Q-DLTS sample under two bias conditions. Left: The band diagram just after the filling pulse. Almost all traps near the oxide interface are filled with electrons. Right: The band diagram after the release of electrons. Most electrons are released from traps in the purple area.

carried out with a bias voltage of -3V , a filling pulse of 6V and a filter rate of 100s^{-1} . In the simulations we used the same settings as for the measurements.

We found we could obtain a good correspondence between the simulated and measured Q-DLTS signal when we assumed a high characteristic energy of the valence band tail (Urbach energy) for a 10nm thick layer at the $\text{SiO}_x/a\text{-Si:H}$ interface. A higher Urbach energy results in higher defect densities according to the defect-pool-model. It is well known that $a\text{-Si:H}$ samples have a highly defective Si layer beneath the native oxide layer with a thickness of approximately 10nm [9]. The parameters used in the simulations are listed in Table I. In this table E_{mob} is the mobility gap, E_{v0} is the Urbach energy, U is the correlation energy, σ is the standard deviation of the Gaussian defect pool and E_p is the position of the peak of the Gaussian defect pool relative to the valence band edge. For the calculation of the emission rates of the single electron states in the valence and conduction band tails we use the parameters e_{00} and E_0 . For

TABLE I
PARAMETER SET FOR THE Q-DLTS SIMULATIONS. THE URBACH ENERGY FOR THE 10nm THICK DEFECTIVE $a\text{-Si:H}$ LAYER AT THE $\text{SiO}_x/a\text{-Si:H}$ INTERFACE IS MARKED WITH *.

parameter	value
E_{mob}	1.75 eV
E_{v0}	$60^*/45$ meV
U	0.27 eV
σ	0.19 eV
E_p	1.18 eV
band tails (single electron states)	
e_{00}	$1.5e9$ s $^{-1}$
E_0	0.07 eV
dangling bonds (amphoteric states)	
$e_{00}^{+/0}$	$1.0e08$ s $^{-1}$
$E_0^{+/0}$	0.06 eV
$e_{00}^{0/-}$	$1.0e10$ s $^{-1}$
$E_0^{0/-}$	0.06 eV

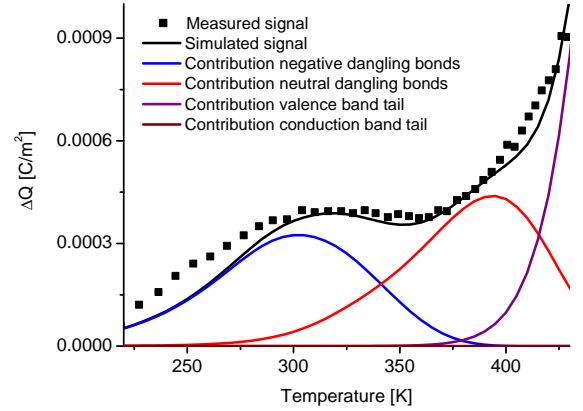


Fig. 5. The measured and simulated Q-DLTS signal.

the emission rates for amphoteric states the parameters e_{00} and E_0 can be adjusted separately for the negatively charged state ($e_{00}^{-/0}$, $E_0^{-/0}$) of the defect and the neutrally charged state ($e_{00}^{0/+}$, $E_0^{0/+}$) of the defect. The Urbach energy for the 10nm thick defective $a\text{-Si:H}$ layer at the $\text{SiO}_x/a\text{-Si:H}$ interface is marked with *.

The measured and simulated Q-DLTS signals are shown in Fig. 5. The figure also shows the contribution of the band tails and the contribution of the amphoteric defects in the negative state and in the neutral state. Note that negatively charged amphoteric states become neutral after the emission of one electron.

Fig. 6 shows the extracted spatial distribution of the defect concentration (top) and energy distribution of the defect density of states (bottom). The energy distribution of states at the $\text{SiO}_x/a\text{-Si:H}$ interface and in the bulk (400nm from the $\text{SiO}_x/a\text{-$

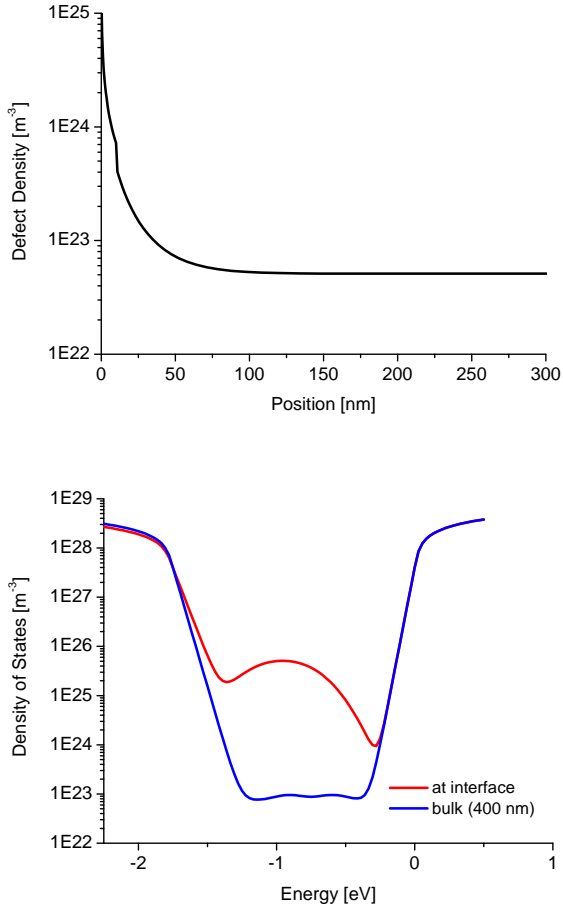


Fig. 6. Top: The defect density versus position as extracted from our simulations for the first 300nm. Bottom: Energy distribution of states at the interface (red line) and 400nm from the interface in the bulk (blue line)

Si:H interface) are plotted.

B. Influence of defect density on the spatial sensitivity of Q-DLTS signals

As the Q-DLTS signal is most sensitive for the region adjacent to the $\text{SiO}_x/a\text{-Si:H}$ interface, the spatial sensitivity of the simulated signal is shown in Fig. 7 for the calibrated parameter set. From this figure it can be seen that, depending on temperature, more than 90% of the signal comes from a region of 100nm wide and more than 60% comes from a region of 10nm wide. The Q-DLTS signal at temperatures below 250°K and at temperatures above 350°K is dominated by a relatively thin region.

Defects near the conduction band and defects near the valence band can only give a significant contribution to the Q-DLTS signal when they are located in a region where the occupation function is shifted over a large range in the bandgap. From the simulated band diagrams in Fig. 8 it can be seen that this is the case only for a relatively thin region adjacent to the $\text{SiO}_x/a\text{-Si:H}$ interface.

To study how severely the highly defective $a\text{-Si:H}$ layer affects the spatial sensitivity, the defect density in this layer was

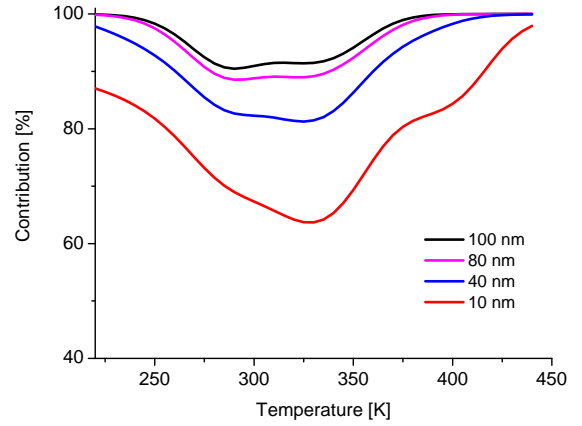


Fig. 7. Spatial sensitivity of the Q-DLTS signal. The contribution of Q-DLTS signal as a function of temperature for several thicknesses (measured from the oxide/semiconductor interface).

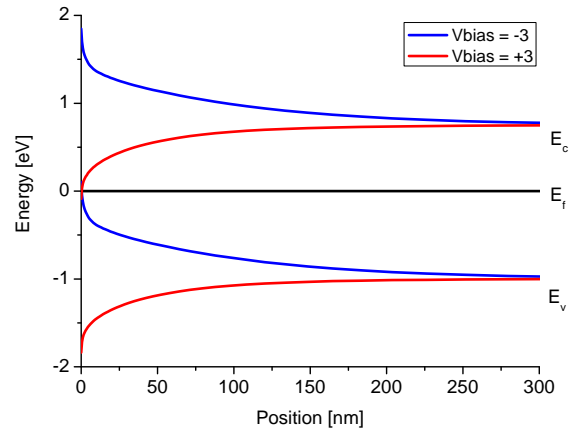


Fig. 8. Band diagrams of the $a\text{-Si:H}$ layer in the MOS structure with a positive and negative bias voltage (+3V and -3V) applied.

varied by changing the Urbach energy. In Fig. 9 the contribution to the Q-DLTS signal of the first 10nm and the first 80nm is shown for several values for the Urbach energy of the first 10nm. From the figure it can be seen that the first 10nm becomes increasingly dominant in the Q-DLTS signal when the Urbach energy increases. It can be seen that for an Urbach energy of 90meV the contribution of the first 10nm exceeds 80%, over the whole temperature range.

IV. CONCLUSIONS

We adapted our device simulator ASA to be able to simulate MIS structures. Using this new version of ASA we can accurately simulate Q-DLTS signals taking into account the spatial distribution of defects, band tail states and amphoteric defect states.

After calibration of the input parameters, good correspondence with experimental results was obtained. In order to get

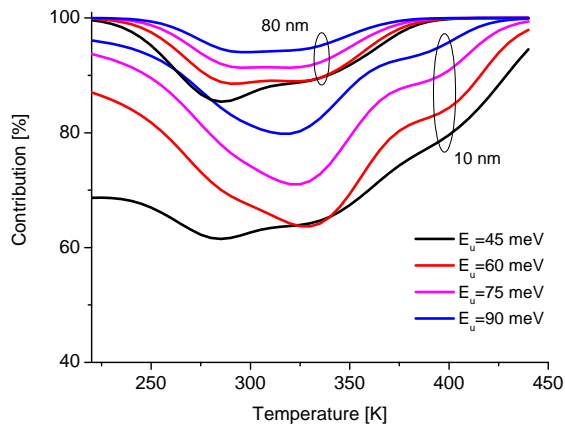


Fig. 9. The spatial sensitivity for several values of the Urbach energy (E_u) for the first 10nm.

a good correspondence between measurements and simulations, we assumed there is a highly defective layer of 10nm thick adjacent to the $\text{SiO}_x/a\text{-Si:H}$ interface. The defect density of the $a\text{-Si:H}$ sample was extracted with the model.

The spatial sensitivity of the Q-DLTS measurement was studied. It was shown that 90% of the the simulated Q-DLTS signal originates from a region less than 100nm wide behind the oxide/semiconductor interface. The Q-DLTS signal originates from the widest region for defects around midgap (corresponding to a temperature range between 250°K and 350°K). The influence of the defective layer adjacent to the $\text{SiO}_x/a\text{-Si:H}$ interface on the spatial sensitivity was studied by varying the Urbach energy in the first 10nm of the $a\text{-Si:H}$ layer. It was found that for an Urbach energy of 90meV the contribution of the first 10nm exceeds 80%, over the whole temperature range.

V. ACKNOWLEDGEMENTS

The authors would like to thank Dr. V. Nádaždy. This work has been funded through the Netherlands Agency for Energy and the Environment (SENTERNOVEM) under contract 2020-01-13-13-002.

REFERENCES

- [1] D. V. Lang, J. D. Cohen, and J. P. Harbison, *Phys. Rev. B* **25**, 5285, 1982
- [2] V. Nadazdy, I. Thurzo, *Phys. Stat. Sol. A* **127**, 167, 1991
- [3] M. Zeman, R. E. I. Schropp, *Amorphous and Microcrystalline Silicon Solar Cells: Modeling, Materials and Device Technology.*, Kluwer Academic Publishers, Boston/Dordrecht/London, 1998, pp 197-199.
- [4] M. J. Powel, S. C. Deane, *Phys. Rev. B* **48**, 10815, 1993
- [5] M. J. Powell and S. C. Deane, *Phys. Rev. B* **53**, 10121, 1996
- [6] G. Schumm, *Phys. Rev. B* **49**, 2427, 1994
- [7] P. Irsigler, D. Wagner, D. J. Dunstan, *J. Phys. C: Solid State Phys.*, **16**, 6605, 1983
- [8] M. Zeman, J.A. Willeman, L.L.A. Vosteen G., Tao, and W.J. Metselaar, *Solar Energy Materials and Solar Cells* **46**, 81, 1997
- [9] H. Yan, A. Morimoto, M. Kumeda, T. Shimizu, and Y Yonezawa, *Mater. Res. Soc. Symp. Proc.* **258**, 247, 1992